Anal. Chem. **2006,** *78,* 7997−8003

Multichannel Reverse Transcription-Polymerase Chain Reaction Microdevice for Rapid Gene Expression and Biomarker Analysis

Nicholas M. Toriello,† Chung N. Liu,‡ and Richard A. Mathies*,†,§

UCSF/UC Berkeley Joint Graduate Group in Bioengineering, Department of Chemical Engineering, and Department of Chemistry, University of California, Berkeley, California 94720

A microdevice is developed for RNA analysis that integrates one-step reverse transcription and 30 cycles of PCR (RT-PCR) amplification with capillary electrophoresis (CE) separation and fluorescence detection of the amplicons. The four-layer glass−PDMS−glass−glass hybrid microdevice integrates microvalves, on-chip heaters and temperature sensors, nanoliter reaction chambers (380 nL), and 5-cm-long CE separation channels. The direct integration of these processes results in attomolar detection sensitivity (<11 template RNA molecules or ~0.1 cellular equiv) and rapid 45-min analysis, while minimizing sample waste and eliminating contamination. Size-based electrophoretic product analysis provides definitive amplicon-size verification and multiplex analysis. Multiplexed differential gene expression analysis is demonstrated on *mdh* and *gyrB E. coli* transcripts. RNA splice variant analysis of the *RBBP8* gene is used to identify tumorigenic tissue. RT-PCR microdevice analysis of normal breast tissue RNA generates the expected 202-bp normal splice isoform; tumor breast tissue RNA samples generate a 151-bp amplicon signifying the presence of the tumorigenic splice variant. The ability to perform RNA transcript and splice variant biomarker analysis establishes our RT-PCR microdevice as a versatile gene expression platform.

The rapid profiling of gene expression levels and measurement of low-abundance RNA transcripts is essential in fundamental studies of pathogenesis, single-cell assays, developmental biology, and stem cell research.[1−4] Techniques for measuring expression profiles must be robust, specific, and sensitive because transcripts of interest are subject to regulation, to rapid degradation, and are expressed at levels ranging from thousands to a single copy per cell. The approaches currently employed for measuring changes in gene expression include in situ fluorescent labeling and imaging,[5] microarray analysis,[6,7] serial analysis of gene expression,[8] protein separation with immunostaining,[9] T7 antisense RNA amplification,[10] and reverse transcription-PCR (RT-PCR).[11−13] Of these techniques, only RT-PCR is capable of rapidly analyzing expression profiles from multiple genes of interest at the single-cell level with single template molecule sensitivity. However, the practical application of RT-PCR thus far has been limited by amplification inefficiencies and by the lack of integrated sample preparation and highly sensitive analytical detection methodologies. In order to reliably quantify the expression of multiple genes over a large range, an integrated miniaturized and efficient amplification and detection scheme that eliminates RNA contamination, RNA degradation, sample loss, and poor transcript level quantification is needed.

Microfabricated devices are ideally suited for the development of low-volume, integrated systems for high-sensitivity RNA amplification and analysis.[14,15] While there have been a number of reports of nucleic acid amplification and detection on microdevices,[16] only a few have demonstrated amplification and detec-

* Corresponding author. Phone: (510) 642-4192. Fax: (510) 642-3599. E-mail: rich@zinc.cchem.berkeley.edu.

† UCSF/UC Berkeley Joint Graduate Group in Bioengineering.

‡ Department of Chemical Engineering.

§ Department of Chemistry.

(1) Golub, T. R.; Slonim, D. K.; Tamayo, P.; Huard, C.; Gaasenbeek, M.; Mesirov, J. P.; Coller, H.; Loh, M. L.; Downing, J. R.; Caligiuri, M. A.; Bloomfield, C. D.; Lander, E. S. *Science* **1999**, *286*, 531−537.

(2) Bittner, M.; Meitzer, P.; Chen, Y.; Jiang, Y.; Seftor, E.; Hendrix, M.; Radmacher, M.; Simon, R.; Yakhini, Z.; Ben-Dor, A.; Sampas, N.; Dougherty, E.; Wang, E.; Marincola, F.; Gooden, C.; Lueders, J.; Glatfelter, A.; Pollock, P.; Carpten, J.; Gillanders, E.; Leja, D.; Dietrich, K.; Beaudry, C.; Berens, M.; Alberts, D.; Sondak, V.; Hayward, N.; Trent, J. *Nature* **2000**, *406*, 536−540.

(3) Klein, C. A.; Seidl, S.; Petat-Dutter, K.; Offner, S.; Geigl, J. B.; Schmidt-Kittler, O.; Wendler, N.; Passlick, B.; Huber, R. M.; Schlimok, G.; Baeuerle, P. A.; Riethmuller, G. *Nat. Biotechnol.* **2002**, *20*, 387−392.

(4) Todd, R.; Margolin, D. H. *Trends Mol. Med.* **2002**, *8*, 254−257.

(5) Xie, X. S.; Yu, J.; Yang, W. Y. *Science* **2006**, *312*, 228−230.

(6) Lockhart, D. J.; Dong, H. L.; Byrne, M. C.; Follettie, M. T.; Gallo, M. V.; Chee, M. S.; Mittmann, M.; Wang, C. W.; Kobayashi, M.; Horton, H.; Brown, E. L. *Nat. Biotechnol.* **1996**, *14*, 1675−1680.

(7) Gray, N. S.; Wodicka, L.; Thunnissen, A.; Norman, T. C.; Kwon, S. J.; Espinoza, F. H.; Morgan, D. O.; Barnes, G.; LeClerc, S.; Meijer, L.; Kim, S. H.; Lockhart, D. J.; Schultz, P. G. *Science* **1998**, *281*, 533−538.

(8) Velculescu, V. E.; Vogelstein, B.; Kinzler, K. W. *Trends Genet.* **2000**, *16*, 423−425.

(9) Gorg, A.; Weiss, W.; Dunn, M. J. *Proteomics* **2004**, *4*, 3665−3685.

(10) Eberwine, J.; Yeh, H.; Miyashiro, K.; Cao, Y. X.; Nair, S.; Finnell, R.; Zettel, M.; Coleman, P. *Proc. Natl. Acad. Sci. U. S. A.* **1992**, *89*, 3010−3014.

(11) Rappolee, D. A.; Wang, A.; Mark, D.; Werb, Z. *J. Cell. Biochem.* **1989**, *39*, 1−11.

(12) Peixoto, A.; Monteiro, M.; Rocha, B.; Veiga-Fernandes, H. *Genome Res.* **2004**, *14*, 1938−1947.

(13) Neves, G.; Zucker, J.; Daly, M.; Chess, A. *Nat. Genet.* **2004**, *36*, 240−246.

(14) Lagally, E. T.; Scherer, J. R.; Blazej, R. G.; Toriello, N. M.; Diep, B. A.; Ramchandani, M.; Sensabaugh, G. F.; Riley, L. W.; Mathies, R. A. *Anal. Chem.* **2004**, *76*, 3162−3170.

(15) Liu, C. N.; Toriello, N. M.; Mathies, R. A. *Anal. Chem.* **2006**, *78*, 5474−5479.

(16) Roper, M. G.; Easley, C. J.; Landers, J. P. *Anal. Chem.* **2005**, *77*, 3887−3893.

10.1021/ac061058k CCC: $33.50
Published on Web 10/26/2006

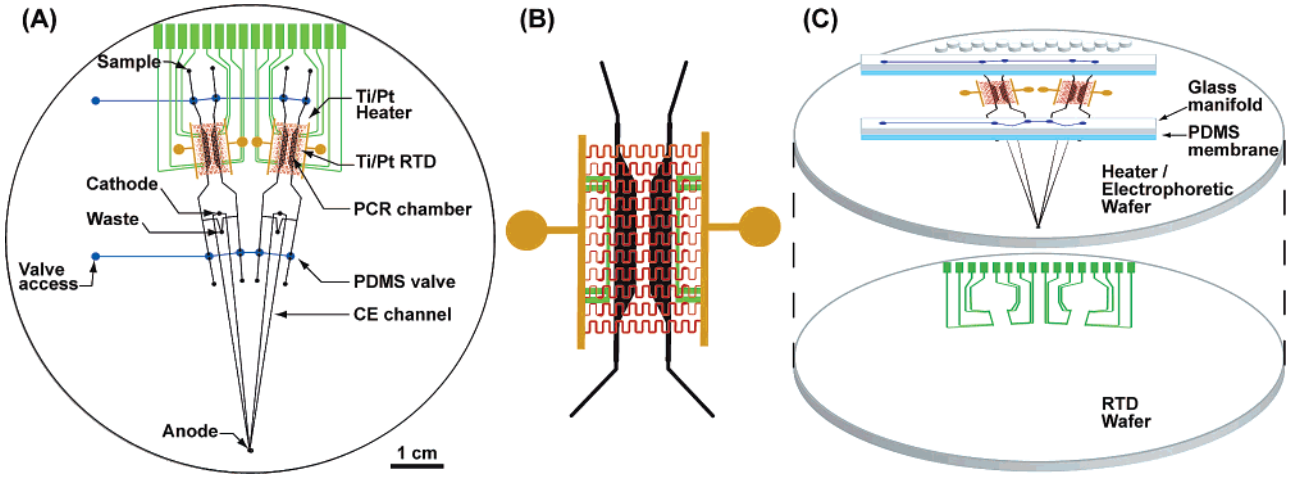

Figure 1. Integrated multichannel RT-PCR microdevice. (A) The microdevice contains two doublet analyzers on a 100-mm-diameter circular wafer. Each of the doublets consists of a resistive heater (red), gold-plated heater leads (brown), Ti/Pt RTDs (green), two reaction chambers, two capillary electrophoresis (CE) separation channels, and PDMS microvalves for fluidic control. (B) An expanded view of the microfabricated reactor region, showing the relative positions of the etched glass reactors, the Ti/Pt heater, and the RTDs. (C) The integrated microdevice is a four-layer glass−PDMS hybrid structure. The topmost wafer is a glass manifold for fluidic actuation. The second layer is a flexible PDMS membrane, which forms the pneumatically actuated microvalves. The glass heater/electrophoresis wafer contains Ti/Pt resistive heaters on the top side along with glass reaction chambers and CE channels etched on the opposite side. The bottom glass RTD wafer contains Ti/Pt temperature-sensing elements.

tionfrom RNA templates.[17−20] Homogeneous real-time RT-PCR amplification was performed using a continuous-flow scheme, but detection was limited to ~10^6 template RNA molecules per reaction.[18] A two-reactor microdevice with valves, temperature sensors, and heaters was developed for RT-PCR amplification from viral RNA.[19] The inability to directly couple amplicon detection resulted in significant sample loss and limited the sensitivity to 1000 starting template copies. A recently developed single-cell RNA extraction microdevice[21] and a homogeneous real-time RT-PCR amplification microdevice[20] show significantly improved limits of detection down to 34 copies. However, the use of homogeneous analysis limits amplicon sizing verification and multiplex analysis. To address these limitations, Zabzdyr and Lillard employed conventional RT-PCR followed by capillary electrophoresis (CE) to analyze highly expressed transcripts in single cells.[22,23] However, employing conventional microliter-scale RT-PCR amplification and nanoliter-scale CE separation results in sample loss, reduced limit of detection, and difficulty in quantitation. Integrating multiplex RT-PCR amplification and electrophoretic analysis in a single microdevice would prevent RNA contamination, degradation, and sample loss, thus improving the reliability and sensitivity of RNA analysis.

To address this challenge, we have developed an integrated multichannel microdevice capable of detecting low RNA transcript levels from multiple genes of interest. The microdevice performs RNA amplification by a one-step RT-PCR process consisting of an isothermal reverse transcriptase reaction, 30 cycles of PCR amplification, and integrated CE separation and detection of the amplified product using laser-induced fluorescence. *Escherichia coli* RNA is used for characterizing the detection sensitivity and multiplex capabilities due to its well-known transcriptome.[24] We also demonstrate successful tumorigenic tissue identification using RNA splice variant analysis.[13,25,26] Both assays establish our RT-PCR microdevice as a versatile platform for fast, parallel, and sensitive biomarker detection.

EXPERIMENTAL SECTION

RT-PCR Microdevice Design. A schematic of the four-layer glass−poly(dimethylsiloxane) (PDMS) multichannel RT-PCR microdevice is shown in Figure 1. Four independently addressable RT-PCR amplification systems are coupled to CE separation channels and arrayed in a symmetrical doublet format on a 100-mm-diameter glass wafer. Each system contains a heater and resistance temperature detector (RTD) for temperature control, PDMS microvalves for fluidic control,[27] a reaction chamber (380 nL), and coupled CE separation channel (5-cm effective length) for parallel RT-PCR amplification and size-based separation of amplicons. The reactor region with the relative positions of the PCR chambers, heaters, and temperature sensing elements are expanded in Figure 1B.

Microfabrication. The RT-PCR microdevice employs similar fabrication procedures used to make previous nucleic acid microdevices.[14,15] Briefly, to form the pneumatic manifold wafer, valve

(17) Anderson, R. C.; Su, X.; Bogdan, G. J.; Fenton, J. *Nucleic Acids Res.* **2000**, *28*, e60.
(18) Obeid, P. J.; Christopoulos, T. K.; Crabtree, H. J.; Backhouse, C. J. *Anal. Chem.* **2003**, *75*, 288−295.
(19) Liao, C. S.; Lee, G. B.; Liu, H. S.; Hsieh, T. M.; Luo, C. H. *Nucleic Acids Res.* **2005**, *33*, e156.
(20) Marcus, J. S.; Anderson, W. F.; Quake, S. R. *Anal. Chem.* **2006**, *78*, 956−958.
(21) Marcus, J. S.; Anderson, W. F.; Quake, S. R. *Anal. Chem.* **2006**, *78*, 3084−3089.
(22) Zabzdyr, J. L.; Lillard, S. J. *Anal. Chem.* **2001**, *73*, 5771−5775.
(23) Zabzdyr, J. L.; Lillard, S. J. *Electrophoresis* **2005**, *26*, 137−145.
(24) Selinger, D. W.; Cheung, K. J.; Mei, R.; Johansson, E. M.; Richmond, C. S.; Blattner, F. R.; Lockhart, D. J.; Church, G. M. *Nat. Biotechnol.* **2000**, *18*, 1262−1268.
(25) Xu, Q.; Lee, C. *Nucleic Acids Res.* **2003**, *31*, 5635−5643.
(26) Wang, Z. N.; Lo, H. S.; Yang, H.; Gere, S.; Hu, Y.; Buetow, K. H.; Lee, M. P. *Cancer Res.* **2003**, *63*, 655−657.
(27) Grover, W. H.; Skelley, A. M.; Liu, C. N.; Lagally, E. T.; Mathies, R. A. *Sens. Actuators, B* **2003**, *89*, 315−323.

Table 1. RT-PCR Primer Sequences

target	sequence	product size (bp)
E. coli gyrB (for)	5′-TCAAGGCGTTCGTTGAATATC-3′	235
E. coli gyrB (rev)	3′-TCTTTGTCCATGTAGGCGTTC-3′	
E. coli mdh (for)	5′-TAAAAACCCAACTGCCTTCAG-3′	204
E. coli mdh (rev)	5′-AACGATCCATACCCGGTTTAC-3′	
human *RBBP8* (for)[a]	5′-AAAGTTTCCAAGTCTTCAACTCATCC-3′	202 (S) and 151 (S′)
human *RBBP8* (rev)	5′-GAGTTTCAGATTCTTCTTGAACACCA-3′	

[a] Human *RBBP8* primer sequences for splice variant analysis from Wang et al.[26]

seats and actuation channels are photolithographically defined and etched to a depth of 38 μm on a 0.55-mm-thick D263 100-mm glass wafer. Valve actuation access holes are drilled, and the manifold is diced into reusable 7 mm × 5 cm strips. Removable PDMS elastomer valves are formed by activating both sides of the 254-μm PDMS membrane with an UV ozone cleaner for 1.5 min, to improve PDMS−glass bonding, and then sandwiching the membrane between the manifold and the bonded channel wafers.

To form the heater/electrophoresis wafer, a 0.55-mm-thick D263 glass wafer is sputter deposited with 200 Å of Ti and 2000 Å of Pt (Ti/Pt) on the top side and with 2000 Å of amorphous silicon on the back side. Heater leads are formed by electroplating gold onto photolithographically defined areas. Ti/Pt serpentine resistive heater elements connecting the gold leads are formed by anisotropically etching photolithographically exposed Ti/Pt in an ion mill. PCR chambers and separation channels are then defined on the back side and etched to a depth of 38 μm. Electrophoresis reservoirs, RTD access holes, and valve via holes are diamond drilled. To form the RTD wafer, a 0.55-mm-thick D263 glass wafer with 2000 Å of Ti/Pt is photolithographically patterned and etched with 90 °C aqua regia to form the 30-μm-wide temperature detection elements and 300-μm-wide leads. The drilled heater/channel wafer is aligned and thermally bonded to the RTD wafer using a programmable vacuum furnace at 580 °C for 6 h. The integrated RT-PCR microdevice requires 50 processing steps including fabrication, drilling, and bonding. The device yield using this fabrication protocol was 100% (n = 3), and each integrated device demonstrated full functionality and no reduction in sensitivity for 100+ amplification and separation cycles. A schematic of the complete fabrication process is available in the Supporting Information (S-3).

RTD Calibration and Thermal Cycling. The four-wire Ti/Pt RTDs are calibrated after thermal bonding as described previously.[14,15] The RTD calibration and representative thermal cycling profile for the RT-PCR microdevice is available in the Supporting Information (S-1 and S-2).

Thermal cycling is controlled through a LabVIEW program with a proportional/integral/differential module. A constant 4-mA source is used to power the RTDs, and the measured voltage from each RTD is collected and filtered using an active low-pass filter. The DAC output then drives the power output from a 0−30 V power supply (GPS-3030DD, Instek, Chino, CA) for the microfabricated heaters at 10 Hz.

***E. coli* RNA RT-PCR Amplification and Capillary Electrophoresis.** Linear polyacrylamide (LPA), 5% (w/v), in 1× Tris TAPS EDTA (TTE) buffer is used as the separation matrix. To suppress electroosmotic flow, the channels are treated with a dynamic coating diluted with methanol (1:1) for 1 min (The Gel Co., San Francisco, CA, DEH-100). The channels are then rinsed with water and acetonitrile and dried completely to ensure bubble-free reagent loading. The loading procedure then begins by filling the separation channels with LPA through the common anode reservoir. The RT-PCR reaction cocktail is then loaded into the empty reaction chamber on a cooled stage (4 °C to minimize RNA degradation) by applying vacuum at the sample waste reservoir. The PDMS elastomer valves are closed after sample introduction by applying 3 psi of pressure to seal the PCR chambers for sample localization and to prevent evaporation during thermal cycling.

RNA reverse transcription, PCR amplification, and CE analysis are performed from an *E. coli* target. A 25-μL RT reaction cocktail comprises Cell-to-cDNA II kit (4 units of M-MLV reverse transcriptase, 0.4 unit of RNase inhibitor, 0.1 μM dNTPs, 1× RT buffer; Ambion Inc., Austin, TX), 2 units of platinum *Taq* DNA polymerase (Invitrogen, Carlsbad, CA), 0.4 μM forward and reverse primers for the *gyrB* gene (IDT, Coralville, IA), and DNase-treated FirstChoice *E. coli* total RNA template (Ambion). Controls without RT and without RNA are performed on the RT-PCR microdevice by removing the M-MLV RT and RNA template from the reaction cocktail, respectively. For the PCR control, *E. coli* RNA template is replaced with 100 *E. coli* K12 MG1655 cells (American Type Culture Collection, Manassas, VA). The *E. coli* cells are transformed with a 3.9-kb PCR 2.1-TOPO vector (Invitrogen) for ampicillin and kanamycin resistance and are grown overnight on ampicillin plates. Colonies exhibiting resistance are picked and grown overnight in autoclaved LB medium containing 25 μg of ampicillin. Cultured *E. coli* K12 cells are washed three times with 1× PBS. Characterization of limit of detection (LOD) for the RT-PCR microdevice is performed from *E. coli* RNA ranging from 10 pg to 1 fg using the same reaction cocktail. Multiplex RT-PCR amplification from *E. coli* RNA is performed using primers directed at the highly conserved *mdh* and *gyrB* genes. Primer sequences are summarized in Table 1.[28]

The thermal cycling protocol employed for all one-step RT-PCR reactions starts with a linear cDNA synthesis from RNA at 42 °C for 15 min using primers complimentary to the RNA transcript of interest. After cDNA synthesis, the M-MLV RT is denatured and the platinum *Taq* polymerase is activated at 95 °C for 60 s followed by 30 cycles of PCR at 95 °C for 5 s, 50 °C for 20 s, and 72 °C for 25 s. Due to the rapid heating (>15 °C s^{-1}) and cooling rates (>10 °C s^{-1}), each cycle of PCR is completed in 50 s and the total reaction time is 41 min.

(28) Taoka, M.; Yamauchi, Y.; Shinkawa, T.; Kaji, H.; Motohashi, W.; Nakayama, H.; Takahashi, N.; Isobe, T. *Mol. Cell. Proteomics* **2004**, *3*, 780−787.

After thermal cycling, the amplified sample is electrophoretically injected and separated in the coupled CE channels. In the first step of the cross injection, the amplified products are injected by applying a 225 V/cm field between the sample and waste reservoir while floating the cathode and anode. Next, a separation field strength of 250 V/cm is applied between the cathode and anode to drive amplified material down the separation column toward the detector. During separation, a back-biasing field of 125 V/cm is applied at the sample and waste for 10 s and then floated for the remainder of the separation. On-column fluorescent labeling of the amplicons occurred during separation by placing 1.3 μM thiazole orange in 1× TTE in the anode and waste reservoirs after thermal cycling to ensure that it does not diffuse into the reaction chamber and inhibit amplification. The electrophoretically separated amplicons are detected using laser-induced fluorescence with the Berkeley rotary confocal scanner providing simultaneous four-color detection from all four separation channels.[29] After each run, the glass manifolds are removed, the PDMS membrane is replaced, and channels and chambers are piranha cleaned to prevent amplicon carryover contamination and RNase accumulation.

Human RNA RT-PCR Amplification for Splice Variant Biomarker Analysis. A 25-μL reaction cocktail for tumor biomarker detection by splice variant analysis is prepared analogous to the *E. coli* RT reaction cocktail. RT-PCR for normal splicing uses 9.5 ng of human breast total RNA (Ambion) and primers directed at the retinoblastoma binding protein 8 (*RBBP8*) (IDT) gene to generate a 202-bp amplicon.[26] Similarly, RT-PCR for tumor specific splicing uses 9.5 ng of human breast tumor RNA (Ambion) and the same primers directed at the *RBBP8* gene to generate a 151-bp amplicons (Table 1).

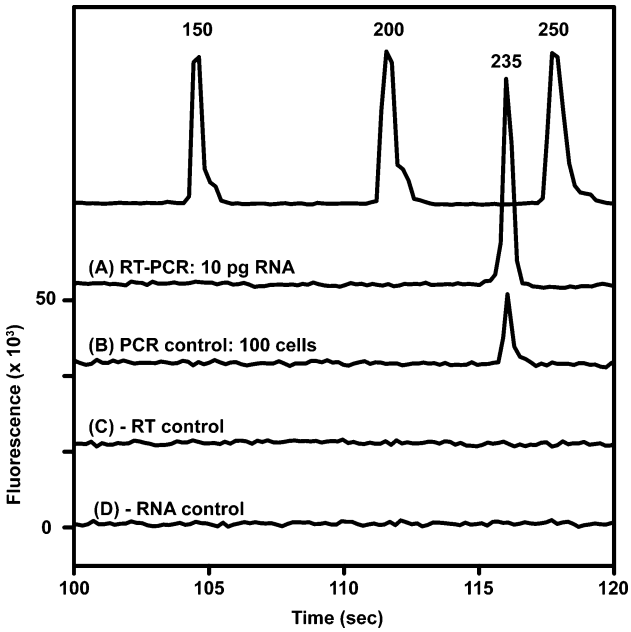

Figure 2. RT-PCR amplification from an *E. coli* target followed by CE analysis on the integrated microdevice. (A) A 235-bp amplicon from the highly conserved *gyrB* gene is detected after RT-PCR amplification from 10 pg of DNase-treated *E. coli* total RNA (~100 cellular equiv) using a one-step RT-PCR amplification. (B) PCR control without DNase treatment and reverse trancriptase performed on 100 *E. coli* cells. (C) Control amplification and analysis of 10 pg of DNase-treated *E. coli* RNA without the reverse transcriptase does not produce a 235-bp band, demonstrating that RNA is the template for the RT-PCR amplification. (D) Control amplification and analysis without RNA to verify that the reaction cocktail does not contain RNA contamination. A 50-bp ladder electropherogram is presented for amplicon sizing reference.

RESULTS AND DISCUSSION

The initial demonstration of RT-PCR and coupled CE analysis on the microdevice is performed from an *E. coli* target. Each 380-nL reactor is loaded at 4 °C with 10 pg of DNase-treated *E. coli* total RNA (~100 cellular equiv) along with the requisite RT-PCR cocktail and primers. One-step RT-PCR amplification is performed from the RNA template in 41 min with primers directed at the highly conserved *gyrB* gene. The subsequent electrophoretic injection and size-based separation on the integrated CE channel yields the expected 235-bp amplicon (Figure 2A). A PCR control on the microdevice directly from 100 *E. coli* cells without reverse transcription followed by CE separation yields a weaker 235-bp amplicon (Figure 2B). The PCR and RT-PCR amplification generate an identical 235-bp fragment because there are no introns in the *E. coli* genome for spliced excision. The greater peak area in the RT-PCR trace (A) compared to the PCR control (B) is due to the increased abundance of *gyrB* transcripts per cell (~118).[28] In Figure 2C, control analysis from 10 pg of DNase-treated *E. coli* RNA without the M-MLV RT produces no product, demonstrating that RNA is the template for the RT-PCR amplification. Similarly, an electropherogram from an analysis without RNA in the reaction cocktail yields no peak (Figure 2D), demonstrating that there is no reagent contamination or carryover. The ability to remove the PDMS microvalves and piranha clean the device after each run ensured that no residual RNA or RNase accumulates in the reactor resulting in template degradation or spurious peak generation.

RT-PCR Microdevice Limit of Detection. The LOD for the RT-PCR microdevice was tested with an *E. coli* RNA template. Electropherograms produced from 10^4, 10^3, 10^2, 10, and 1 fg of RNA template after RT-PCR amplification are presented in Figure 3. The expected 235-bp *gyrB* amplicon is detected from all samples down to 10 fg of total RNA template (S/N = 100). The electropherograms demonstrate the expected correlation between initial template concentration and amplicon peak height, and the LOD is found to be below 10 fg of total *E. coli* RNA. The average *E. coli* cell contains ~100 fg of RNA, and the transcript of interest in this study, *gyrB*, is only present at ~118 copies/cell or less than 0.2% of the total RNA by mass.[24,28] The successful amplification and detection from 10 fg of RNA demonstrates the RT-PCR microdevice is capable of analyzing single cells (~0.1 cellular equiv) and low copy number transcripts (<11 copies/reactor). While the S/N ratio for 10 fg of RNA (~11 copies) suggests that significantly lower limits of detection should be achievable, stochastic effects resulted in irreproducible amplification and detection at the 1 fg of RNA limit.

Our RT-PCR microdevice shows significant improvement over previously reported RNA analysis systems that could not amplify from labile RNA template[16,30] and superior integration to those that do not couple on-chip RNA amplification[18−20] and size-based

(29) Shi, Y. N.; Simpson, P. C.; Scherer, J. R.; Wexler, D.; Skibola, C.; Smith, M. T.; Mathies, R. A. *Anal. Chem.* **1999**, *71*, 5354−5361.

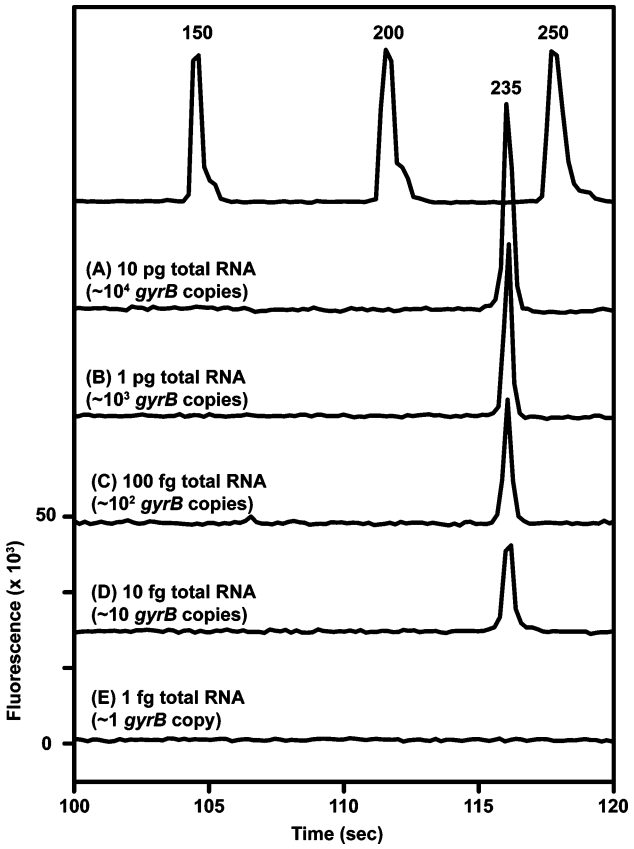

Figure 3. Characterization of LOD for the RT-PCR microdevice. (A) Reverse transcription, 30 cycles of PCR amplification and CE analysis of a 235-bp fragment of the *gyrB* gene in the *E. coli* transcriptome is performed on 10 pg of total RNA (~11 000 template molecules) in a 380-nL microreactor in 41 min. In traces B−E, companion analysis is performed on 1 pg, 100 fg, 10 fg, and 1 fg of RNA in the reactor corresponding to 10^3, 10^2, 10, and 1 *gyrB* RNA template molecules, respectively. A 50-bp ladder electropherogram is presented for amplicon sizing reference.

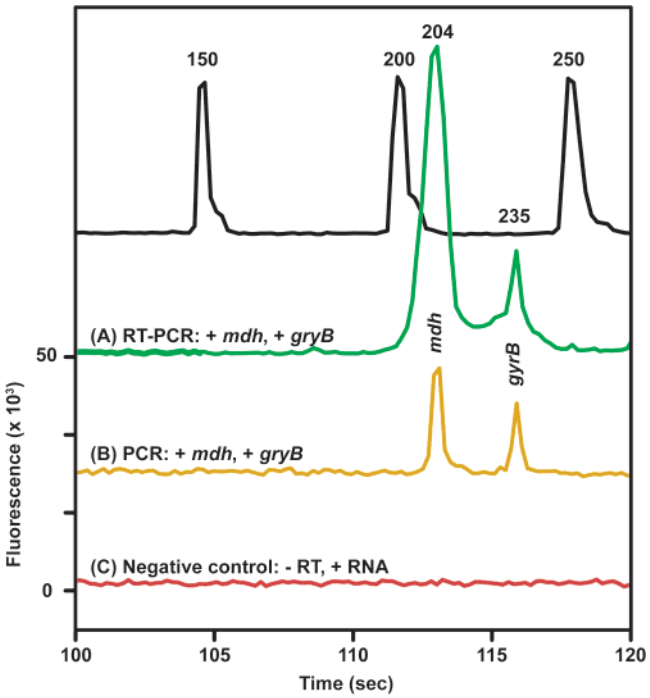

Figure 4. Analysis of relative transcript abundance levels using multiplex RT-PCR amplification. (A) One-step multiplex RT-PCR amplification from 10 pg (~100 cellular equiv) of DNase-treated *E. coli* RNA with primers specific to the *mdh* and *gyrB* genes. (B) Multiplex PCR amplification from 100 *E. coli* cells without RT produces the *mdh* and *gyrB* amplicons with the expected 1:1 ratio. (C) Control RT-PCR experiment on 10 pg of DNase-treated *E. coli* RNA with primers for *mdh* and *gyrB* gene but no RT.

separation for fragment size verification.[23,31] Previously reported RNA analysis techniques with manually integrated sample preparation, amplification, and detection require labor-intensive amplification protocols for low template copy analysis. These protocols include (1) separate cDNA synthesis and PCR amplification (two-step RT-PCR), (2) an excess of 35 amplification cycles, or (3) two separate rounds of PCR amplification with nested primers. The one-step RT-PCR protocol utilized in our microdevice is far less demanding. The primary drawback to the one-step RT-PCR process is the lower amplification efficiency due to the mutually antagonistic buffering conditions for reverse transcriptase (high $[Mn^{2+}]$) and *taq* polymerase (high $[Mg^{2+}]$).[23] Despite the reduced amplification efficiency caused by this factor, our microdevice outperforms other RNA analysis microdevices, which reported detection limits of ~10^6, 10^3, and 34 template RNA molecules.[18−20] The ability to directly couple low reactor volume (380 nL) amplification with CE on this robust integrated microdevice minimizes sample loss and eliminates contamination thereby enabling reproducible low copy number RNA amplification and detection.

While our RT-PCR microdevice shows excellent sensitivity, there is still significant room for improvement. The cross-injection scheme offers precise metering of amplicon loading, but is wasteful (<1% injection efficiency) and limits our ability to quantitatively correlate amplicon peak area with starting template copy number. Due to the limited amount of amplified material in the 380-nL microreactor, injection timing is a critical parameter. The inconsistent cross-injection timing is primarily a result of run-to-run variation in the placement of the reactor−gel interface. The redesigned injection arm used here shows significant improvement over our previous multichannel PCR-CE design;[15] however, future work is aimed at optimizing the CE injection further through direct-injection methods.[32,33]

Multiplex RT-PCR for Gene Expression Analysis. Multiplex RT-PCR offers a platform for evaluating relative changes in gene expression profiles and understanding the interplay of gene transcripts in both normal and diseased tissue. A multiplex RT-PCR amplification was performed from 10 pg (~100 cellular equiv) of DNase-treated *E. coli* RNA with primers specific to the *mdh* and *gyrB* genes. This analysis produced 204- and 235-bp amplicons (Figure 4A), whose intensities correctly reflect the enhanced (4×) abundance of *mdh* transcripts relative to *gyrB*. Multiplex PCR

(30) Pal, R.; Yang, M.; Lin, R.; Johnson, B. N.; Srivastava, N.; Razzacki, S. Z.; Chomistek, K. J.; Heldsinger, D. C.; Haque, R. M.; Ugaz, V. M.; Thwar, P. K.; Chen, Z.; Alfano, K.; Yim, M. B.; Krishnan, M.; Fuller, A. O.; Larson, R. G.; Burke, D. T.; Burns, M. A. *Lab Chip* **2005**, *5*, 1024−1032.
(31) Zabzdyr, J. L.; Lillard, S. J. *Anal. Chem.* **2002**, *74*, 1857−1862.
(32) Paegel, B. M.; Yeung, S. H. I.; Mathies, R. A. *Anal. Chem.* **2002**, *74*, 5092−5098.
(33) Blazej, R. G.; Kumaresan, P.; Mathies, R. A. *Proc. Natl. Acad. Sci. U. S. A.* **2006**, *103*, 7240−7245.

without reverse transcriptase from 100 *E. coli* cells generates the *mdh* and *gyrB* amplicons from DNA with the expected 1:1 ratio (Figure 4B). A separate control from 10 pg of DNase-treated *E. coli* RNA with primers for the *mdh* and *gyrB* genes but no reverse transcriptase generates no amplicon. Thus, the RT-PCR microdevice demonstrates specific amplification from two transcripts of interest in a mixed population of *E. coli* RNA and properly reports on the relative abundance of each.

Many RT-PCR schemes employ homogeneous analysis of the products because it is fast and easy to implement. However, homogeneous multiplex amplification and detection schemes are limited by the overlap of the different fluorescent labels employed. Additionally, homogeneous analysis does not directly permit size-based verification of the products, which is useful because RNA is highly regulated and undergoes rapid degradation and in some higher level organisms alternative splicing. CE analysis coupled to RT-PCR amplification on the microdevice allows for (1) efficient low-volume transfer of amplified material and (2) the ability to perform a quantitative size-based separation of multiple RNA transcripts to verify proper identification and to improve multiplexing.

Tumor Biomarker Detection by Splice Variant Analysis. Tumor-associated alternative RNA splicing isoforms may have clinical significance for point-of-care disease diagnostics.[25,26,34,35] When cells become tumorigenic, many genes show a change in their splicing pattern, resulting in the (1) complete shift from one splice isoform to another, (2) loss of one splice form in tumors, or (3) upregulation of the tumor splice variant. Those genes showing a binary switch from normal to tumor-specific splicing have potential as diagnostic biomarkers for cancer. A fast and robust system for analyzing shifts in spicing patterns could have significant clinical impact. For this reason, we performed splice variant analysis from human tissue RNA on the integrated RT-PCR microdevice.

The *RBBP8* gene is used as a tumor biomarker in this study because of its central role in *BRCA1* suppression under normal growth conditions. In tumorigenic tissue, the *RBBP8* gene undergoes a shift in its splicing pattern (S to S') generating a transcript that is 51 bp shorter in length (Figure 5 top). To detect this change, primers are designed to amplify from the *RBBP8* gene on either side of the splice site.[26] The normal splicing (S) of this gene will result in the excision of all introns and ligation of all three exon subunits to generate a 202-bp fragment, while tumor-specific splicing (S') will result in the removal of all introns and the middle exon, generating a 151-bp amplicon. As shown in Figure 5A, RT-PCR amplification and subsequent electrophoretic separation from 9.5 ng of normal breast tissue RNA generates the expected 202-bp amplicon. The tumor breast tissue RNA sample generates both the 202-bp and the 151-bp splice variant amplicons because it is likely excised from tissue that contains a mixture of normal and tumorigenic cells (Figure 5B). To confirm the results, a PCR control without RT was performed on the DNase-treated RNA tissue samples. Both the normal and tumor-specific RNA produce no amplicons.

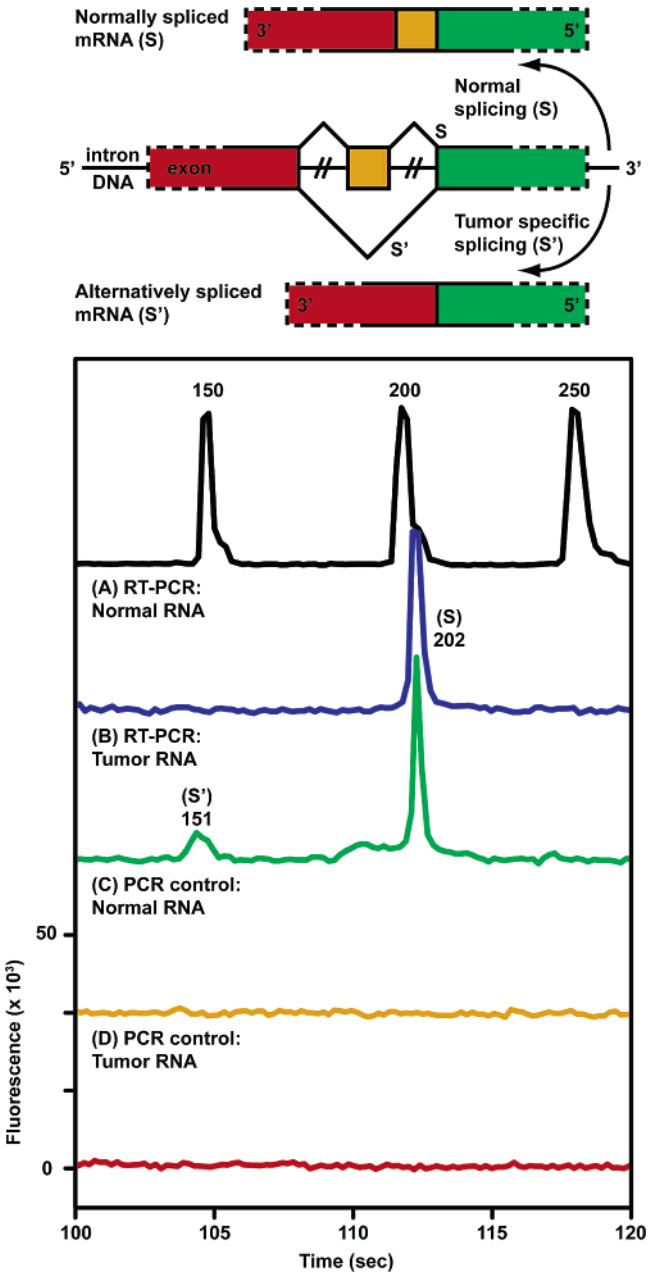

Figure 5. (Top) Schematic of normal *RBBP8* splicing (S) compared to tumor-specific splicing (S'). Solid bars indicated exons, and the bridging lines indicate two alternative splice pathways. Normal splicing of the *RBBP8* gene results in intron removal and ligation of all three subunits. A tumor-specific splice variant is generated by the removal of introns and the middle exon subunit (yellow), resulting in a shorter mRNA transcript. (Bottom) Tumor biomarker detection by splice variant analysis with the RT-PCR microdevice. (A) The *RBBP8* gene from 9.5 ng of breast tissue RNA is amplified using the RT-PCR protocol and analyzed with the microdevice. Normal breast tissue RNA produces a single amplicon (202 bp) representative of normal mRNA splicing. (B) Tumor breast tissue RNA produces two amplicons: the expected 202-bp product and the 151-bp tumor specific splice variant product. A PCR control performed without RT on the DNase-treated normal (C) and tumor (D) breast tissue RNA validates that we are seeing RNA amplification.

Coupling size-based CE analysis to RNA amplification on the RT-PCR microdevice provides a platform for tumor biomarker detection from only 9.5 ng of RNA in <45 min using splicing variant analysis. The integrated amplification and detection micro-

(34) Saito, H.; Nakatsuru, S.; Inazawa, J.; Nishihira, T.; Park, J. G.; Nakamura, Y. *Oncogene* **1997**, *14*, 617−621.
(35) Correa, R. G.; de Carvalho, A. F.; Pinheiro, N. A.; Simpson, A. J. G.; de Souza, S. J. *Genomics* **2000**, *65*, 299−302.

device is faster and more sensitive than any commercially available system. Coupling of this system with laser capture microdissection or needle biopsy would provide a fast, sensitive, and low-volume analysis system for near real-time biomarker genetic analysis.[4]

SUMMARY AND CONCLUSIONS

A parallel fully integrated RT-PCR microdevice has been developed to perform one-step reverse transcription and amplification from attomolar (low copy number) amounts of RNA in submicroliter (380 nL) volumes followed by the direct electrophoretic separation and detection of the RT-PCR amplicons in <45 min. The microdevice demonstrates sensitivity down to 11 initial RNA copies or 0.1 cellular equiv with only 30 PCR cycles, suggesting it will be an excellent platform for single-cell gene expression analysis. Successful multiplex RT-PCR illustrates that the microdevice is also capable of determining relative transcript abundance levels for gene expression profiling and can be employed for RNA genotyping from heterogeneous samples. The potential of this instrument for cancer biomarker detection by splice variant analysis is also demonstrated.

This highly sensitive four-channel array RT-PCR microdevice lays the foundation for an integrated highly parallel RNA analysis microsystem. Injection process optimization using affinity-capture purification should result in a 10-fold detection sensitivity improvement and a concomitant increase in quantitation capabilities.[32,33] This improved injection efficiency along with recently developed directed single-cell capture[36,37] should enable single RNA transcript sensitivity and provide a platform for quantitative single-cell gene expression profiling. Integrating this multiplex RNA analysis system with our portable microsystem technologies[14,38] should also lead to a powerful tool for point-of-care diagnostics and real-time viral detection and genotyping.

(36) Toriello, N. M.; Douglas, E. S.; Mathies, R. A. *Anal. Chem.* **2005**, *77*, 6935−6941.
(37) Chandra, R. A.; Douglas, E. S.; Mathies, R. A.; Bertozzi, C. R.; Francis, M. B. *Angew. Chem., Int. Ed.* **2006**, *45*, 896−901.
(38) Skelley, A. M.; Scherer, J. R.; Aubrey, A. D.; Grover, W. H.; Ivester, R. H. C.; Ehrenfreund, P.; Grunthaner, F. J.; Bada, J. L.; Mathies, R. A. *Proc. Natl. Acad. Sci. U. S. A.* **2005**, *102*, 1041−1046.

ACKNOWLEDGMENT

We thank Robert Blazej and Erik Douglas for valuable discussions. N.M.T. and C.N.L. were supported by a NIH Molecular Biophysics Training Grant (T32GM08295) and Chevron-Texaco Graduate Fellowship, respectively. Microfabrication was performed in the UC Berkeley Microfabrication Laboratory. This work was supported by NIH grants R01HG01399 and HG003329 and by the Chemical Sciences Division of the U.S. Department of Energy under contract DE-AC03-76SF00098.

SUPPORTING INFORMATION AVAILABLE

Additional information as noted in text. This material is available free of charge via the Internet at http://pubs.acs.org.

Received for review June 9, 2006. Accepted September 9, 2006.

AC061058K